Quantitative measurements of *CH** concentration in normal gravity and microgravity coflow laminar diffusion flames

D. Giassi[1], S. Cao[1], D. P. Stocker[2], F. Takahashi[3], B. A. Bennett[1], M. D. Smooke[1], M. B. Long[1]

[1] Department of Mechanical Engineering and Materials Science, Yale University
[2] NASA Glenn Research Center
[3]National Center for Space Exploration Research

Keywords: *CH** chemiluminescence, SLICE coflow flames, microgravity

With the conclusion of the SLICE campaign aboard the ISS in 2012, a large amount of data was made available for the analysis of the effect of microgravity on laminar coflow diffusion flames. Previous work focused on the study of sooty flames in microgravity as well as the ability of numerical models to predict its formation in a simplified buoyancy-free environment. The current work shifts the investigation to soot-free flames, putting an emphasis on the chemiluminescence emission from electronically excited *CH* (*CH**). This radical species is of significant interest in combustion studies: it has been shown that the *CH** spatial distribution is indicative of the flame front position and, given the relatively simple diagnostic involved with its measurement, several works have been done trying to understand the ability of *CH** chemiluminescence to predict the total and local flame heat release rate. In this work, a subset of the SLICE nitrogen-diluted methane flames has been considered, and the effect of fuel and coflow velocity on *CH** concentration is discussed and compared with both normal gravity results and numerical simulations. Experimentally, the spectral characterization of the DSLR color camera used to acquire the flame images allowed the signal collected by the blue channel to be considered representative of the *CH** emission centered around 431 nm. Due to the axisymmetric flame structure, an Abel deconvolution of the line-of-sight chemiluminescence was used to obtain the radial intensity profile and, thanks to an absolute light intensity calibration, a quantification of the *CH** concentration was possible. Results show that, in microgravity, the maximum flame *CH** concentration increases with the coflow velocity, but it is weakly dependent on the fuel velocity; normal gravity flames, if not lifted, tend to follow the same trend, albeit with different peak concentrations. Comparisons with numerical simulations display reasonably good agreement between measured and computed flame lengths and radii, and it is shown that the integrated *CH** emission scales proportionally to the computed total heat release rate; the two-dimensional *CH** spatial distribution, however, does not appear to be a good marker for the local heat release rate.

The authors gratefully acknowledge NASA for the support under cooperative agreement NNX11AP43A.

Quantitative Measurements of *CH** Concentration in Normal Gravity and Microgravity Coflow Laminar Diffusion Flames

D. Giassi[1], S. Cao[2], D.P. Stocker[3], F. Takahashi[4], B.A.V. Bennett[1], M.D. Smooke[1], M.B. Long[1]

(1) Yale University; (2) GE Global Research; (3) NASA Glenn Research Center; (4) Case Western Reserve University

Introduction and Motivation

Due to the lack of buoyancy effects, microgravity flame experiments have several advantages over their normal gravity counterparts:

- The simplified flow field provides easier test cases to refine computational models.
- Microgravity allows the creation of flame conditions that do not exist on Earth and enables study near flame extinction.

In this work, we extend the microgravity investigation from the characterization of sooty flames [1] to the quantification of the *CH** radical in non-sooty nitrogen-diluted coflow laminar diffusion flames. *CH** chemiluminescence is responsible for most of the blue appearance of flames (like the diffusion flame shown in Fig. 1), and it is recognized as an important marker for both flame structure and heat release rate.

Fig. 1: Example of blue chemiluminescent emission from a nitrogen-diluted methane diffusion flame

SLICE (*Structure and Liftoff in Combustion Experiments*)

- SLICE was an experimental campaign conducted on the International Space Station in 2012.
- One of the objectives was the investigation of the influence of microgravity on the structure of coflow laminar diffusion flames.

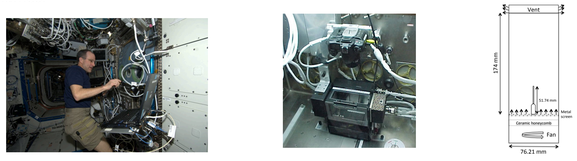

Fig.2: Astronaut Don Pettit running SLICE experiments on board the ISS (left); the SLICE hardware inside the Microgravity Science Glovebox (center); schematic of the SLICE burner (right).

- Several flame configurations have been studied by varying operational parameters such as fuel nozzle diameter, fuel type, and dilution, as well as flow velocities. Current work focused on the following conditions:

Case	Fuel nozzle I.D.	Fuel type (N_2 diluted)	Flow velocity
A	3.2 mm	40% CH_4	Fuel: 17 to 89 cm/s Coflow air: 17 cm/s
B	1.6 mm	70% CH_4	Fuel: 62 cm/s Coflow air: 14 to 34 cm/s

- SLICE was a preliminary series of experiments done to support the CLDFlame (Coflow Laminar Diffusion Flame) experiment, which is part of the future ACME campaign (*Advanced Combustion via Microgravity Experiments*), expected in 2017.
- The principal SLICE diagnostic tool was a Nikon D300s DSLR camera (see Fig. 1-center), calibrated and spectrally characterized to perform quantitative measurements (soot temperature, soot volume fraction measurements, and *CH** radical concentration).

DSLR Camera Characterization

- Conventional chemiluminescence measurements rely on an interference filter to isolate and collect the light emitted by a specific radical species.
- The spectral characterization of the color camera allowed the signal collected by the blue channel to be considered representative of the *CH** emission of the $A^2\Delta \rightarrow X^2\Pi$ transition centered around 431 nm.
- Preliminary measurements, performed on a well characterized nitrogen-diluted 65% methane reference flame, showed good agreement between the normalized radial chemiluminescent profiles obtained from the Nikon blue channel and a 430 nm interference filter (Fig. 3-left).
- Figure 3-right shows the normalized transmissivities of a Nikon CFA blue filter and a 430 nm interference filter, when compared to the spectral location of relevant chemiluminescent species: the broadband blue filter is expected to collect light from emitting species other than *CH**, such as C_2* and CO_2*.

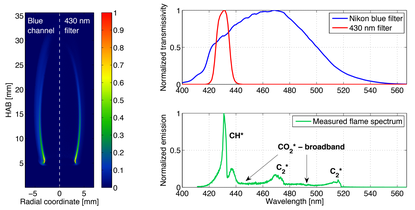

Fig. 3: Comparison between radial flame chemiluminescence collected by the Nikon blue filter and a 430 nm interference filter (left); normalized Nikon blue filter and 430 nm interference filter transmissivities, compared to spectral emission of flame chemiluminescent species (right).

Imaging Considerations

- In flames with an axisymmetric structure, the radial chemiluminescence profile is obtained from the line-of-sight emission through the use of an Abel deconvolution, a process that assumes the collected rays to be parallel.
- For a given distance between the light source and the collection optics, the smaller the lens *f*-number, the weaker the parallel rays hypothesis becomes; as a consequence the reconstructed radial profile gets artificially broadened (as demonstrated in Fig. 4), and the peak value underestimated.
- To maximize signal level while minimizing exposure time (thus fuel consumption), the SLICE images were taken with a relatively small *f*-number of 2 or 4.

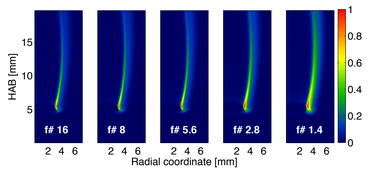

Fig.4: Influence of lens *f*-number on the Abel-inverted normalized radial chemiluminescence of the reference nitrogen-diluted 65% methane flame.

Spectral Considerations

- For the accuracy of the quantitative measurement, it is essential that the collected chemiluminescence is related only to the radical species of interest.
- The effect of C_2* and CO_2* emission on the collected signal was evaluated following a spectral characterization of the reference 65% methane flame. Figure 5a shows the flame spectrum collected at 7.5 mm above the burner; the horizontal and vertical axes identify the radial and spectral coordinates, respectively. The white lines demarcate the FWHM spectral width of a 430 nm interference filter, while the Nikon blue filter covers the entire range.
- Figure 5b shows the normalized radial profile of the flame chemiluminescence. The curves are obtained by spectrally integrating over the 430 nm filter and blue filter spectral regions of Fig. 5a. The integration over the entire spectral range, due to the C_2* and CO_2* contribution, yields a broader radial profile and explains the halo seen in Fig. 3-left.
- The radial peaks of C_2* and *CH** are not coincident; when the two species are spectrally integrated, as is the case for the blue channel acquisition, the radial distance of the peak *CH** from the flame centerline is expected to be underestimated. In the current work, however, the system magnification was such that the effect was negligible.

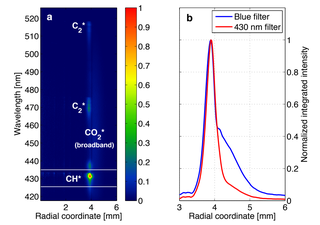

Fig. 5: (a) Normalized spectrum as function of the radial coordinate (7.5 mm HAB) for the reference 65% methane flame. (b) Normalized radial profiles obtained by integrating over the 430 nm and blue filter spectral regions.

- The additional light emitted by C_2* and CO_2* will increase the recorded counts. If not corrected, this would result in an overestimation of the actual *CH** signal; a comparison between the chemiluminescence collected by the blue channel and a 430 nm interference filter showed that the detected signal in the blue channel, regardless of the axial position, is greater by a nearly constant factor of ~3.3, as shown in Fig. 6. (The 430 nm filter signal has been corrected to account for the partial transmissivity of the filter.)

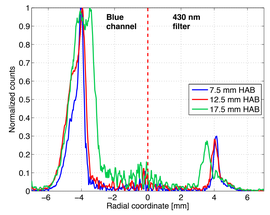

Fig. 6: Comparison between the normalized radial chemiluminescence, as collected by the blue channel and 430 nm interference filter for three heights above the burner.

- In cases where the flow conditions are such that the flame becomes partially sooty (see Fig. 7a), the blue channel will detect signal from soot incandescence as well, causing additional corruption of the real *CH** signal. In the normalized blue channel shown in Fig. 7b, the wing signal can be associated with the *CH** emission, while the tip is mainly due to soot luminosity.
- A method to account for soot luminosity relies on the use of additional information that can obtained from the camera's green channel (Fig. 7c). Blue and green signals are normalized with respect to their maxima along the wings; since no soot is present along the wings, the two normalized images are subtracted to obtain one that has just the soot contribution on the tip (Fig. 7d). The resulting image is then scaled to match the tip peak intensity of the blue channel, and subtracted from the original blue signal to obtain a "soot-free" blue image (Fig. 7e).

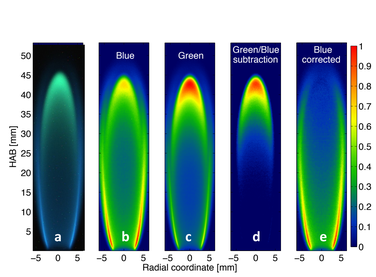

Fig. 7: (a) Color image of a representative partially sooty flame; (b, c) normalized line-of-sight luminosity as collected by the blue and green channels; (d) soot luminosity as determined by the green/blue subtraction; (e) flame's blue signal free of soot interference.

*CH** Concentration Diagnostics

- The collected *CH** emission signal S_{em} can be related to the number density N^* according to Eq. 1 [2]:

$$S_{em} = \frac{1}{4\pi} A_{21} \tau V_{em} N^* K \qquad (1)$$

- A_{21}: Einstein A coefficient (1.86e6 s^{-1})
- τ: exposure time
- V_{em}: pixel volume
- K: calibration constant

- In the SLICE setup, the calibration constant *K* was determined using a heated 100 μm *SiC* fiber; the fiber-emitted radiation was imaged with the camera and, thanks to the known fiber emissivity, its temperature was evaluated using color ratio pyrometry [3]. The ratio between the measured fiber signal and the calculated fiber intensity (as collected by the blue channel at the self-measured temperature *T*) provided a value for the intensity calibration, as in Eq. 2.

$$K = \frac{B}{\tau \int_{\lambda_1}^{\lambda_2} \eta_B(\lambda)\varepsilon(\lambda) I_{BB}(\lambda,T)\, d\lambda} \cdot C \cdot \gamma_{CH} \qquad (2)$$

- η_b: blue filter spectral transmissivity
- ε: fiber emissivity (ε=0.88)
- I_{BB}: blackbody radiation
- B: measured *SiC* fiber signal
- $\lambda_1 - \lambda_2$: blue filter detection wavelength range

- The constant *C* considered the contribution of emitting species other than *CH**, while the term γ_{CH} is the transmitted energy of a photon in the blue channel, as in Eq. 3.

$$\gamma_{CH} = \int_{\lambda_1}^{\lambda_2} \eta_B(\lambda) \frac{hc}{\lambda} CH_{em}(\lambda)\, d\lambda \qquad (3)$$

- h: Planck's constant
- c: speed of light
- Ch_{em}: normalized *CH** spectral emission (numerically obtained from the molecular software LIFBASE [5])

[1] B. Ma, S. Cao, D. Giassi, D. P. Stocker, F. Takahashi, B. A. Bennett, M. D. Smooke, M. B. Long, Proc. Comb. Inst. 35, 839-846 (2015)
[2] H. M. Hertz, G. W. Faris, Opt. Lett. 13, 351-353 (1988)
[3] P. B. Kuhn, B. Ma, B. C. Connelly, M. D. Smooke, M. B. Long, Proc. Comb. Inst. 33, 743-750 (2011)
[4] K. T. Walsh, J. Fielding, M. D. Smooke, M. B. Long, A. Liñan, Proc. Comb. Inst. 30, 357-365 (2005)
[5] J. Luque, D. R. Crosley, "LIFBASE: database and spectral simulation", SRI International Report MP 99-009 (1999)
[6] S. Cao, B. A. Bennett, M. D. Smooke, Comb. Theory and Model. - to appear - (2015)
[7] www.me.berkeley.edu/gri_mech/

Supported by NASA under cooperative agreement NNX11AP43A.

Results

- The procedure to compute the *CH** concentration was initially tested on the 65% reference methane flame (for which previous concentration measurements are available [4]), and it displayed good quantitative agreement (Fig. 8). The mole fraction value shown in Fig. 8 was obtained from the number density, assuming a temperature of 1900 K.
- The uncertainty in the determination of the *SiC* fiber temperature (±30 K) can translate into a maximum uncertainty in the absolute *CH** concentration of roughly 40%.

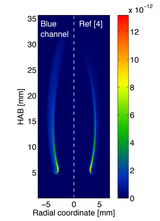

Fig. 8: *CH** mole fraction of the target 65% methane flame (left half), as compared to the result from [4] (right half).

- Figure 9-left shows the absolute *CH** concentration spatial distribution for the flames of *Case A*: the fuel flow is increased as the coflow is maintained constant. The left half of each image displays the microgravity result, while the right half shows the normal gravity one. The peak *CH** concentration of both normal gravity and microgravity flames (Fig. 9-right) is seen to be weakly dependent and relatively insensitive to the fuel velocity.

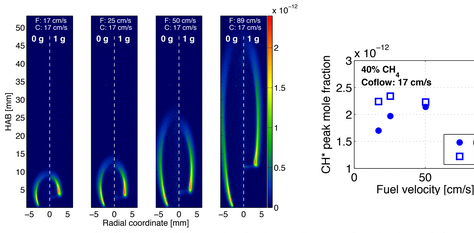

Fig. 9: Absolute *CH** mole fraction for the flames of *Case A* (left); variation of the peak *CH** concentration as function of fuel flow (right).

- Figure 10-left shows the absolute *CH** concentration spatial distribution for the flames of *Case B*: the coflow is increased as the fuel flow is maintained constant. For this configuration, the peak *CH** concentration of both microgravity and normal gravity flames (Fig. 10-right) shows a dependence on the coflow velocity.

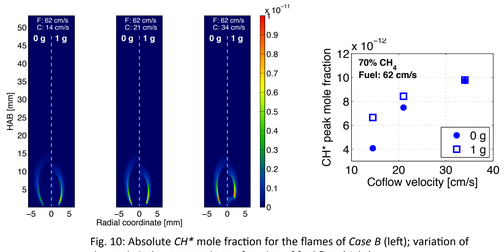

Fig. 10: Absolute *CH** mole fraction for the flames of *Case B* (left); variation of the peak *CH** concentration as function of fuel flow (right).

- The computational model implemented to simulate the SLICE diffusion flames is based on the MC-Smooth vorticity-velocity formulation of the governing equations [6]; the gas chemistry is described by 42 species and 250 reactions, and it is based on the GRI 3.0 mechanism [7]. The resulting coupled and nonlinear equations are solved using a modified Newton's method with a Bi-CGSTAB linear solver.
- Figure 11 shows the comparison between the integrated *CH** absolute concentration in a cross section, and the integrated computed heat release rate for *Cases A* and *B*. The correlation between the two quantities is seen to be excellent, confirming that the total *CH** chemiluminescence can be a useful marker for the total flame heat release rate in laminar coflow diffusion flames.

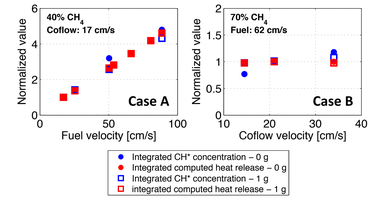

Fig. 11: Normalized integrated radial *CH** concentration and integrated heat release rate for the two cases considered.

- Figure 12-left displays the comparison between the normalized radial *CH** concentration distribution and the normalized local heat release rate for a representative flame of *Case A*. Despite minor differences in flame structure, the spatial distribution of the two quantities is similar and both follow the position of the flame front. On the other hand, the gradients and intensities do not match; in Fig. 12-right the normalized radially integrated counts of *CH** concentration and heat release rate are plotted as functions of the flame's axial coordinate, demonstrating the difference between *CH** and heat release rate spatial gradients.

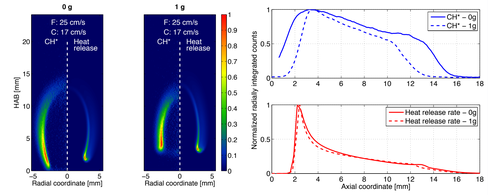

Fig. 12: Comparison between normalized two-dimensional radial *CH** concentration and computed two-dimensional heat release rate for a selected flame from *Case A* (left); comparison between the radially integrated normalized *CH** and heat release rate (right).

Conclusions

- Quantitative measurements of *CH** concentration have been performed on selected microgravity and normal gravity SLICE flames.
- The spectral characterization of the SLICE color camera allowed the blue channel signal to be considered representative of the *CH** emission around 431 nm.
- A reference diffusion flame was spectrally analyzed to investigate the contribution of chemiluminescent species other than *CH**, and used to verify the validity of the proposed approach.
- The measured peak *CH** concentration displayed a higher sensitivity to coflow variations than to fuel flow variations, and was generally higher in normal gravity.
- It was shown that, for laminar coflow diffusion flames, the integrated radial absolute *CH** concentration scales proportionally to the simulated integrated flame heat release rate.
- The two-dimensional *CH** and heat release rate distributions agree reasonably well, but the variations in spatial intensities and gradients do not match.